Electronic Supplementary Material (ESI) for Journal of Materials Chemistry A.

Supplementary Information for

EDTA-Mimic Amino Acid-Metal Ions Coordination for Multifunctional Packings

Kai Tao, Asuka A. Orr, Wen Hu, Pandeeswar Makam, Jiahao Zhang, Qiang Geng, Boxin Li, Joseph M. Jakubowski, Yancheng Wang, Phanourios Tamamis, Rusen Yang, Deqing Mei, Ehud Gazit

Table S1. Appearance of the Gla solution after mixing with diverse metal ions

No.	Metal ions	Atomic No. in the Element Table	Appearance
1	Mg^{2+}	12	A few floc precipitates
2	Al^{3+}	13	A few floc precipitates
3	Ca^{2+}	20	Transparent solution
4	Fe^{3+}	26	Many floc precipitates
5	Co^{2+}	27	A few floc precipitates
6	Cu^{2+}	29	Blue needle-like crystals
7	Zn^{2+}	30	White needle-like crystals
8	Ga^{3+}	31	Many floc precipitates
9	Cd^{2+}	48	A few floc precipitates
10	La^{3+}	57	Many floc precipitates
11	Ce^{3+}	58	Many floc precipitates
12	Nd^{3+}	60	Many floc precipitates
13	Tb^{3+}	65	A few floc precipitates
14	Ir^{3+}	77	A few floc precipitates
15	Bi^{3+}	82	Many floc precipitates

Note: the concentrations of Gla and metal ions were fixed at 5.0 mM and 10.0 mM, respectively. The solution pH was adjusted to 4.0 ± 0.2.

The results demonstrated that most of the tested metal ions could complex with Gla molecules and organize into superstructures which precipitated once reaching sufficient size, thus demonstrating that Gla can act as an omnipotent bio-chelator.

Table S2. Probabilities of branching between "ladder, antiparallel" and "step, head-tail" networks within the analysed simulation snapshots

No. of Gla in a "ladder, antiparallel" or "step, head-tail" network	Probability of branching of a "ladder, antiparallel" with a "step, head-tail" network	Probability of branching of a "step, head-tail" with a "ladder, antiparallel" network
3	0.24	0.08
4	0.52	0.37
5	0.67	0.32
6	0.68	0.22
7	0.81	0.15
8	0.76	0.25

Note: Clusters 3-8 molecules in size were focused on since these clusters are more complex than isolated pairs of Gla molecules and are populated enough for statistical significance. Larger clusters were omitted as they do not occur frequently enough for statistical significance.

Table S3. Metal ion coordinates examined in this work and their crystal structure parameters

Item	Crystal parameters	CCDC
EDTA+Ag(I)	P 1-triclinic a= 14.6625 Å b= 5.8491 Å c= 14.4190 Å α=90.7542° β=127.3282° γ=69.8607° V=890.94 Å^3 Z=2	2039400
Gla+Zn(II)	P $2_12_12_1$-orthorhombic a=14.3089 Å b=9.2594 Å c=7.2872 Å a/b=1.5453 b/c=1.2706 c/a=0.5093 V=965.49 Å^3 Z=4	2039399
Gla+Cu(II)	P $2_12_12_1$-orthorhombic a=9.2403 Å b=14.2629 Å c=7.1967 Å a/b=0.6479 b/c=1.9819 c/a=0.7788 V=948.48 Å^3 Z=4	2039398

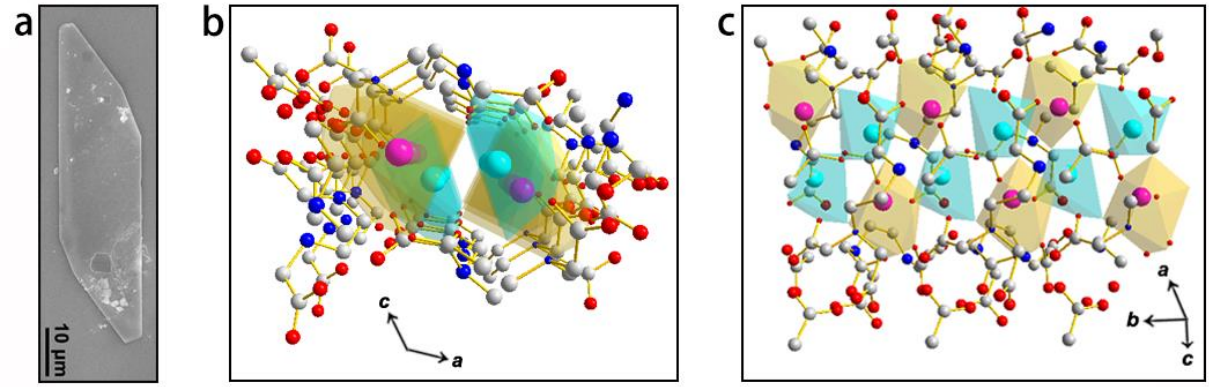

Fig. S1 Structural characterization of the EDTA+Ag(I) coordination crystals. a, SEM image of the plate-like crystals. **b, c,** Crystallographic structures along the (**b**) transection and (**c**) longitudinal direction of the crystals. The carbon, nitrogen, oxygen and silver atoms are represented as grey, blue, red and cyan (magenta) spheres, respectively. The hydrogen atoms are omitted for clarity.

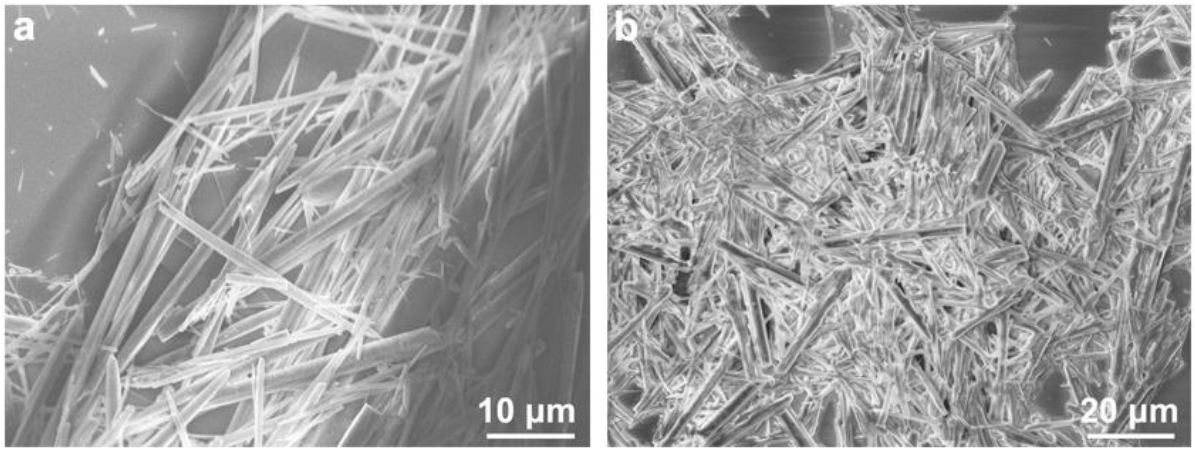

Fig. S2 SEM images of the Gla-metal ions chelation crystals after heating at 80 ºC for 1 h. a, Gla+Cu(II). **b**, Gla+Zn(II).

The results demonstrated that the bio-coordinated assemblies were quite thermostable and kept intact at high temperatures, in contrast to pristine amino acids/peptides crystals.

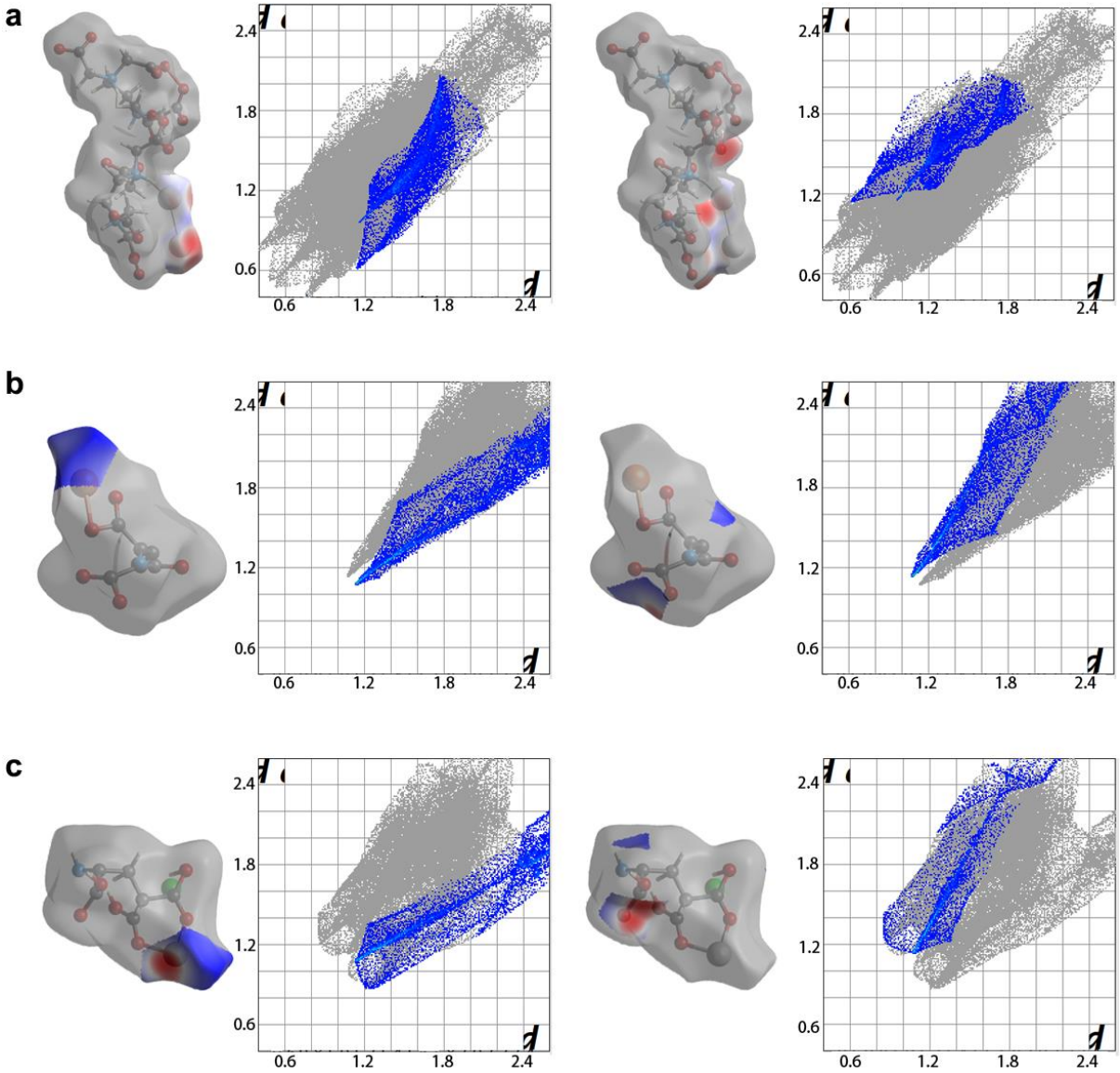

Fig. S3 Hirshfeld surface and 2D fingerprint plots of the coordinates. a, EDTA+Ag(I). **b**, Gla+Cu(II). **c**, Gla+Zn(II). In each item, the left and right panels show the highlight close contacts of $Metal_{inside}$-$All_{outside}$ and All_{inside}-$Metal_{outside}$, respectively.

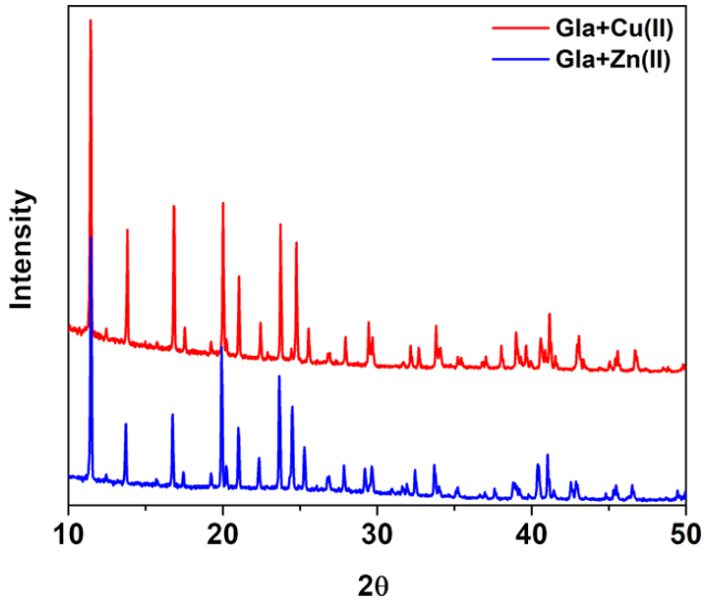

Fig. S4 XRD spectra of Gla+Cu(II) and Gla+Zn(II). Gla+Cu(II) and Gla+Zn(II) crystals showed the same XRD profiles, demonstrating their identical molecular structures, consistent with the crystallographic characterizations.

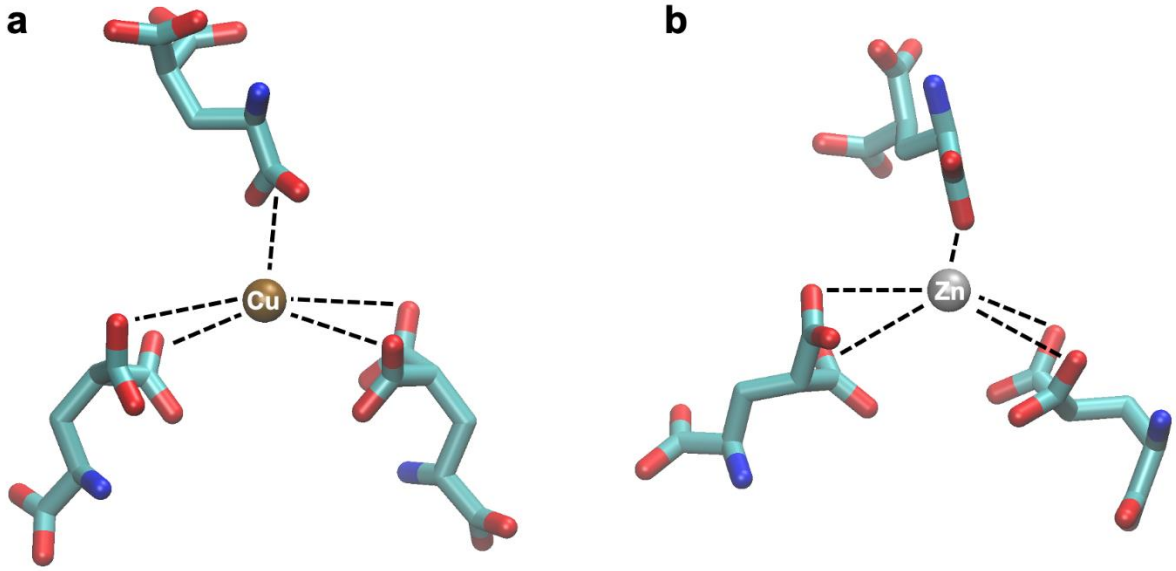

Fig. S5 Simulated coordination structures of metal ions with Gla molecules. a, Gla+Cu(II). **b,** Gla+Zn(II). The results demonstrated that the Gla+Cu(II) and Gla+Zn(II) systems had the same coordination structures, consistent with the experimental findings. Additional simulations of Gla+Zn(II) were performed and are not presented in detail in this study.

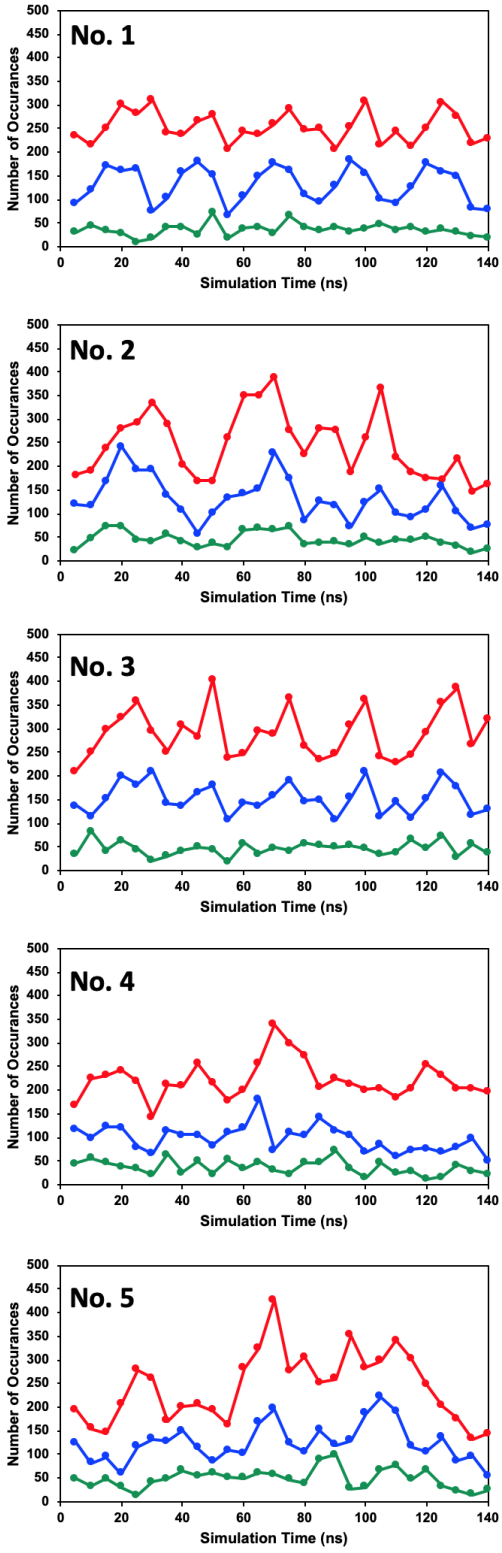

Fig. S6 Number of occurrences of interactions between Gla molecules over 5 simulation runs. "Ladder, antiparallel" interactions (red), "step, head-tail" interactions (blue), "step, antiparallel" interactions (green), averaged every 5 ns per simulation trajectory. Interactions formed between pairs of Gla molecules are shown, whether they are part of a network or not.

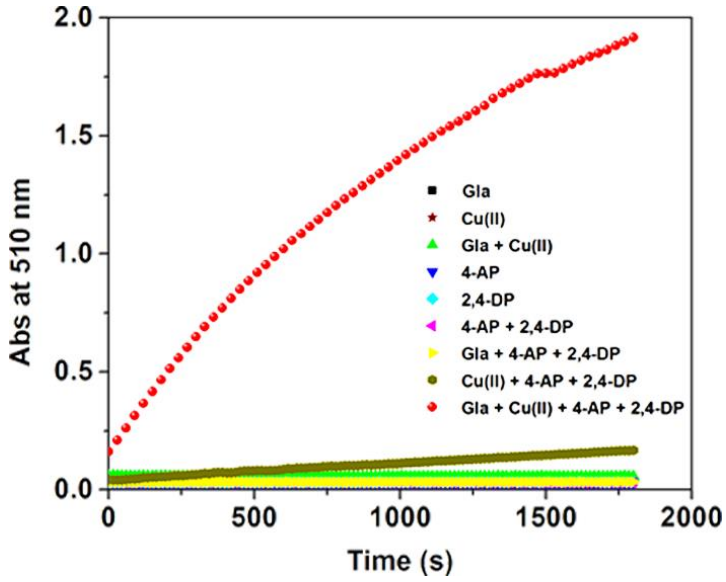

Fig. S7 The coupling reaction of 2,4-DP and 4-AP in the presence of different catalyst combinations as monitored over time.

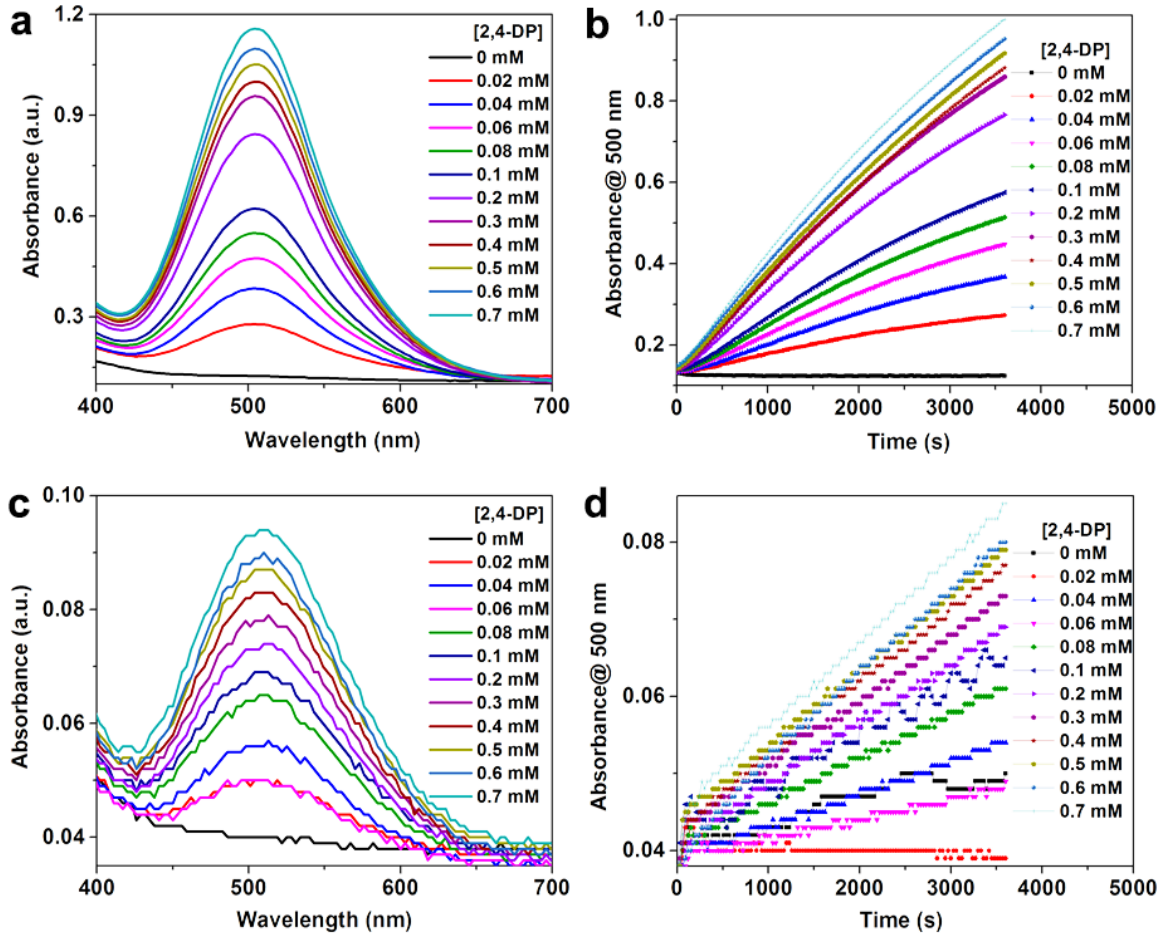

Fig. S8 UV-vis absorption of 2,4-DP and 4-AP mixed solution catalysed by (a, b) Gla+Cu(II) and (c, d) laccase. **a** and **c**, UV-vis absorption spectra of the reaction solution versus the concentration of 2,4-DP. **b** and **d,** The 507 nm absorption of the reaction solution at different concentrations of 2,4-DP as monitored over time. In all experiments, [4-AP] = 0.1 mg mL^{-1}.

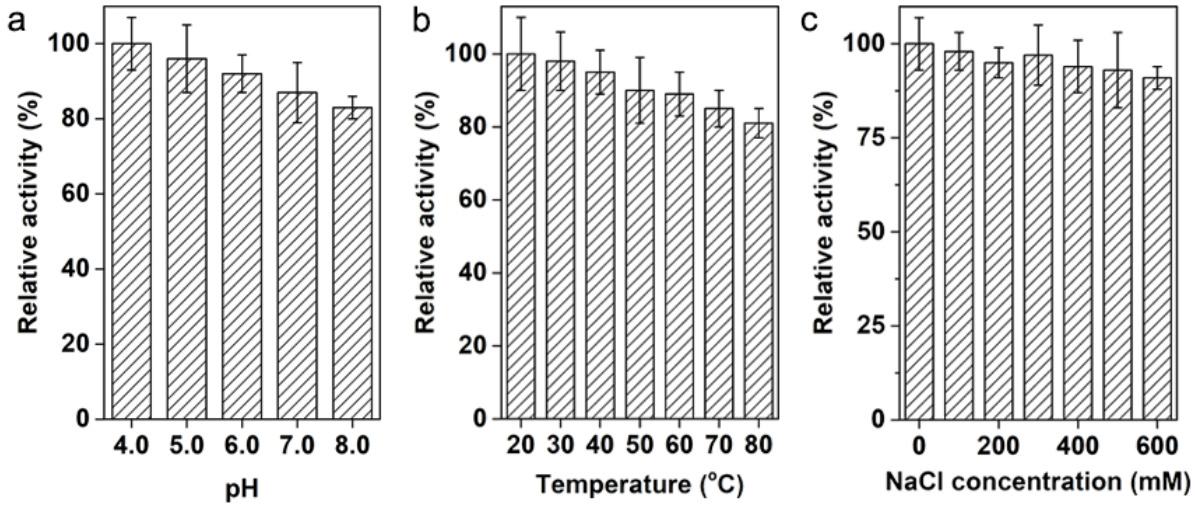

Fig. S9 Catalytic stability of Gla+Cu(II) crystals at different (a) pH values, (b) temperatures and (c) NaCl concentrations. In all experiments, [Gla+Cu(II)] = 0.1 mg mL^{-1}, [4-AP] = 0.1 mg mL^{-1}.

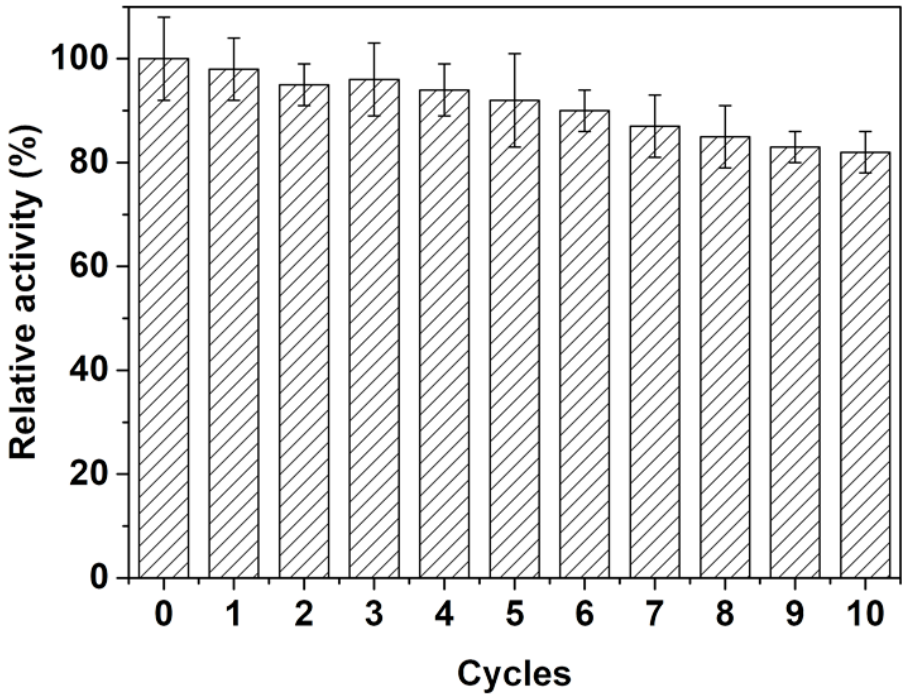

Fig. S10 Relative catalytic activity of Gla+Cu(II) in the chromogenic reaction during recycling and reuse. In all experiments, [Gla+Cu(II)] = 0.1 mg mL^{-1}, [4-AP] = 0.1 mg mL^{-1}.

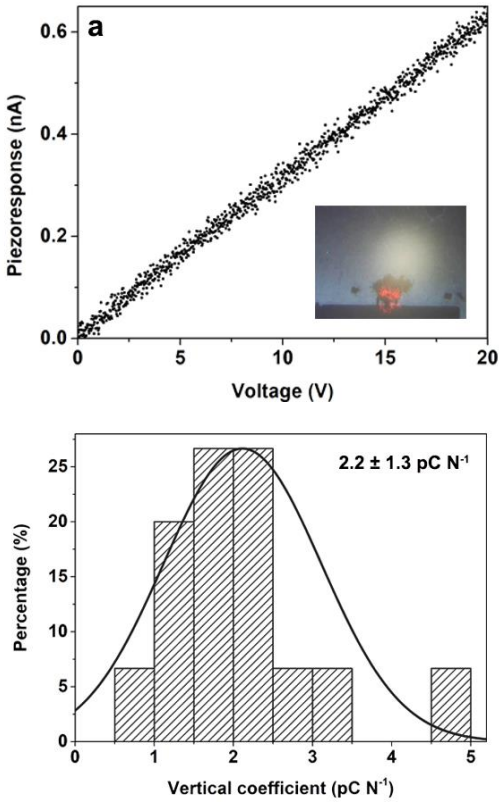

Fig. S11 Piezoelectric coefficient measurements of Gla+Zn(II) crystals using PFM. a, Linear relationship between the piezo-response as measured by the photodiode system versus the applied voltage. The inset shows a representative microscopy photograph of the sample during characterization. **b**, Statistical distribution of the vertical coefficients of Gla+Zn(II) crystals measured using PFM, showing a statistical vertical coefficient of 2.2 ± 1.3 pC N^{-1}. For accuracy, a total of 75 counts were used for statistical analysis.

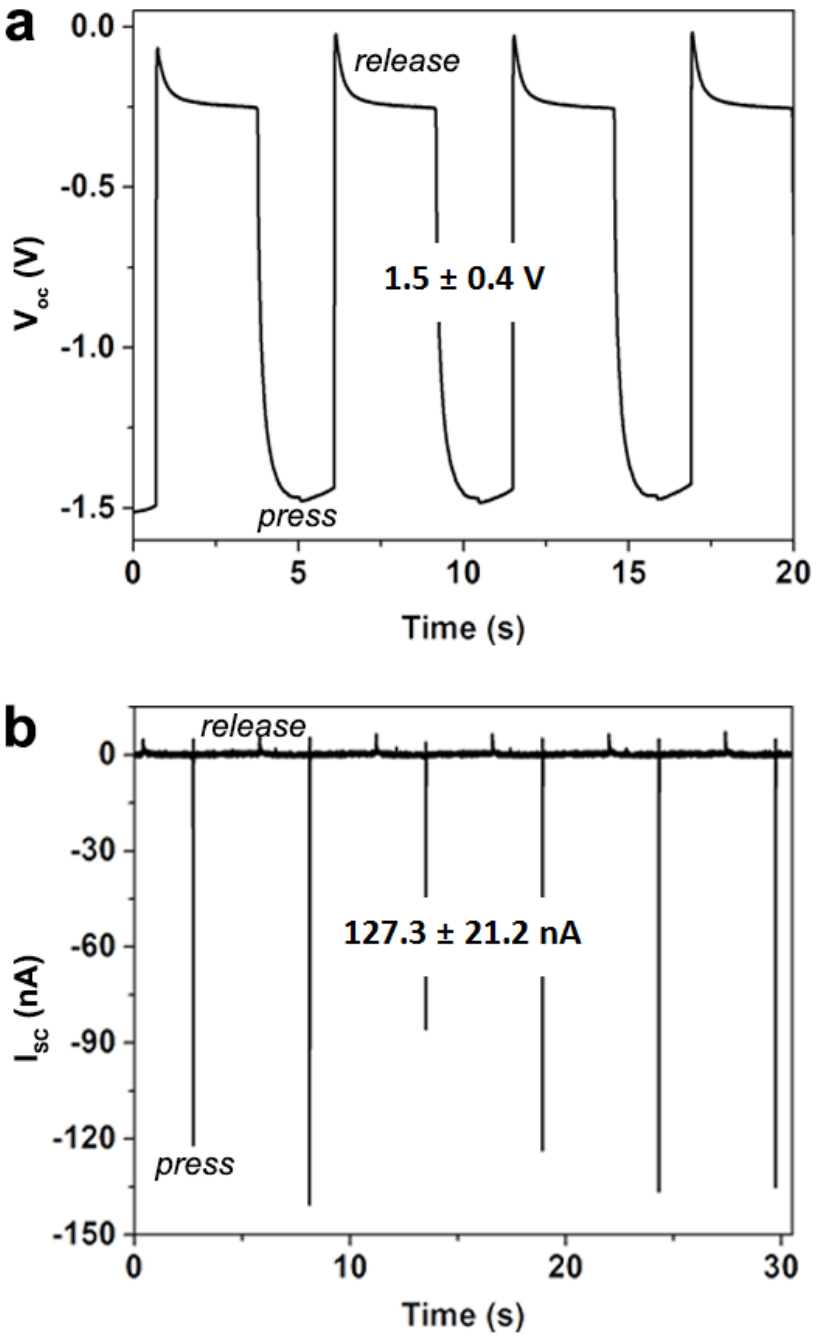

Fig. S12 Signal outputs from the generator shown in Fig. 3a in the main text after switching the connection. a, Open-circuit voltage. **b**, Short-circuit current.